The Hydrogen-Bonded 2-Pyridone Dimer Model System. 1. Combined NMR and FT-IR Spectroscopy Study

Łukasz Szyc,[†] Jing Guo,[‡] Ming Yang,[†] Jens Dreyer,[†] Peter M. Tolstoy,[‡] Erik T. J. Nibbering,*[,†] Bogusława Czarnik-Matusewicz,[§] Thomas Elsaesser,[†] and Hans-Heinrich Limbach[‡]

Max Born Institut für Nichtlineare Optik und Kurzzeitspektroskopie, Max Born Strasse 2A, D-12489 Berlin, Germany, Institut für Chemie und Biochemie, Freie Universität Berlin, Takustrasse 3, D-14195 Berlin, Germany, and Faculty of Chemistry, University of Wrocław, F. Joliot-Curie 14, 50-383 Wrocław, Poland

Received: April 22, 2010; Revised Manuscript Received: June 08, 2010

2-Pyridone (PD), converting to 2-hydroxypyridine (HP) through a lactam−lactim isomerization mechanism, can form three different cyclic dimers by hydrogen bond formation: $(PD)_2$, (PD−HP), and $(HP)_2$. We investigate the complexation chemistry of pyridone in dichloromethane-d_2 using a combined NMR and Fourier transform infrared (FT-IR) approach. Temperature-dependent ^{1}H NMR spectra indicate that at low temperatures (<200 K) pyridone in solution predominantly exists as a cyclic $(PD)_2$ dimer, in exchange with PD monomers. At higher temperatures a proton exchange mechanism sets in, leading to a collapse of the doublet of ^{15}N labeled 2-pyridone. Linear FT-IR spectra indicate the existence of several pyridone species, where, however, a straightforward interpretation is hampered by extensive spectral overlap of many vibrational transitions in both the fingerprint and the NH/OH stretching regions. Two-dimensional IR correlation spectroscopy applied on concentration-dependent and temperature-dependent data sets reveals the existence of the $(PD)_2$ cyclic dimer, of PD−CD_2Cl_2 solute−solvent complexes, and of PD−PD chainlike dimers. Regarding the difference in effective time scales of the NMR and FT-IR experiments, milliseconds vs (sub)picoseconds, the cyclic dimers (PD−HP) and $(HP)_2$, and the chainlike conformations HP−PD, may function as intermediates in reaction pathways through which the protons exchange between PD units in cyclic $(PD)_2$.

1. Introduction

One of the key structural motifs in DNA and RNA are the hydrogen-bonded nucleotide pairs. To understand the high replication yield of DNA, hydrogen bonding between DNA bases and the possibility of proton transfer within a base pair have been the topic of numerous studies.[1−9] To avoid the complexity of macromolecular structures containing a stack of hydrogen-bonded base pairs, basic investigations often focus on single dimers in the gas phase or in solution. Frequently, the naturally occurring nucleobases are further simplified by replacing them by model systems.[10−13] For instance, 2-pyridone (PD) has been used as a model for the pyrimidines uracil or thymine.[12,14] The cyclic amide PD is subject to lactam−lactim tautomerism, whereby 2-hydroxypyridine (HP) is formed (Scheme 1). In the gas phase both HP and PD have been investigated, as isolated molecule[15−17] or in clusters with water or ammonia[18−22] or larger hydrogen bonding agents.[23,24] In the solid state hydrogen-bonded puckered chains of PD with orthorhombic lattice type are predominant.[25,26] In a recent study an alternative monoclinic polymorph with cyclic dimer units has been reported.[27] In solution, however, both tautomers occur because of relatively small energy differences, with the equilibrium depending sensitively on solvent properties. As PD has a larger dipole moment than HP, PD is favored in polar (protic) solution, whereas HP is favored in nonpolar (aprotic) solvents.

Both tautomers can dimerize to form three possible combinations, the two cyclic homodimers $(PD)_2$ and $(HP)_2$, and the cyclic mixed dimer (PD-HP) (Scheme 1). Gas phase experiments allow detailed aspects of particular dimers to be investigated independently.[19,20,28−33] In solution, however, the two cyclic homodimers and the cyclic mixed dimer have been suggested to appear simultaneously.[34−39] In hydrogen bonding solvents the two monomer tautomers can also form complexes with solvent

SCHEME 1

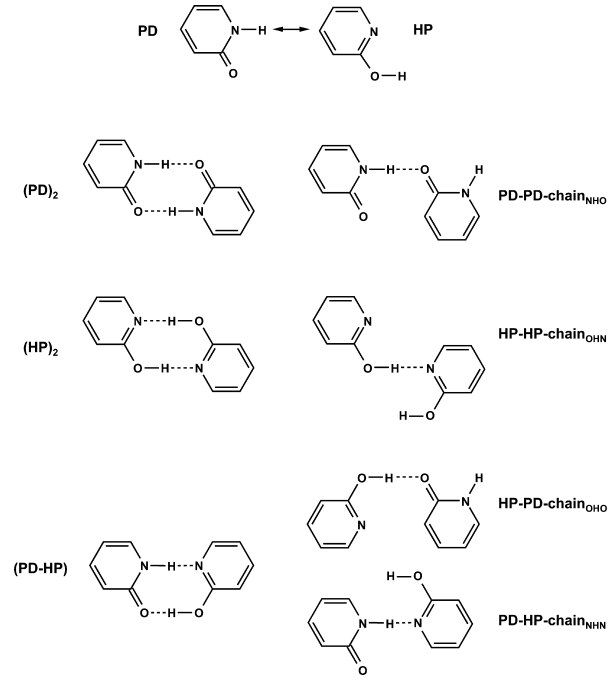

* Corresponding author, nibberin@mbi-berlin.de.
[†] Max Born Institut für Nichtlineare Optik und Kurzzeitspektroskopie.
[‡] Institut für Chemie und Biochemie, Freie Universität Berlin.
[§] Faculty of Chemistry, University of Wrocław.

10.1021/jp103630w
Published on Web 07/01/2010

SCHEME 2

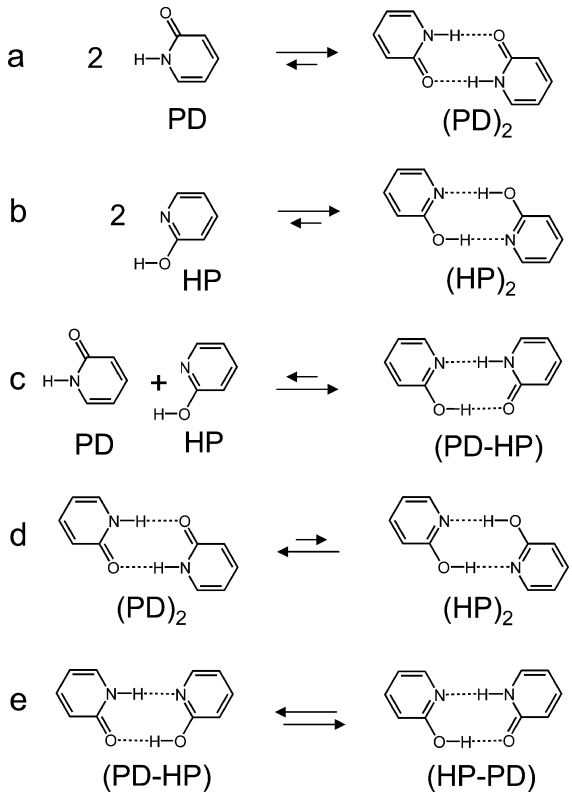

molecules. In addition, the presence of chainlike dimeric species containing only a single hydrogen bond between the monomers should be taken into account. As a result, a variety of solvent-dependent equilibria determine the relative concentrations of the different species. Their multitude makes it cumbersome to determine all equilibrium constants, which until now has mostly been attempted by means of UV,[34−36,38,40−42] IR,[37,38,43−46] and NMR spectroscopy[38,42,47] or by theoretical methods.[39,45,47−51] IR spectroscopy has been used to derive structural information on gas phase PD or HP monomer by looking at the free NH or OH stretching band[52] or at the full spectrum of PD using fluorescence dip spectroscopy[33] and on PD in solution by use of ^{15}N and ^{18}O isotope labeling.[53] $(PD)_2$ and (PD−HP) dimers in the gas phase have been explored with fluorescence dip spectroscopy.[19,20,31,32] In liquid solution fingerprint modes have been assigned to either PD monomer or cyclic $(PD)_2$,[37] and experimental low temperature matrix isolation spectroscopy of PD and HP has also been reported,[43,44] as well as theoretical studies analyzing these results.[45,54,55] The low-frequency intermolecular modes of $(PD)_2$ have also been studied in detail in gas phase experiments,[28−30,56] in liquid solution,[57] and with theoretical methods.[58]

In the complexation chemistry of PD/HP, hydrogen bonds play a central role. Proton transfer, necessary to convert PD into HP or vice versa, can be mediated by hydrogen bonds in protic solvents (Scheme 2). In particular the two cyclic homodimers may exchange by a double proton tranfser mechanism, converting $(PD)_2$ into $(HP)_2$, and vice versa, through the double hydrogen bond coordinate. Proton transfer in the cyclic mixed dimer, changing (PD−HP) into (HP−PD), has been investigated in light of possible proton transfer between DNA bases.[59]

Generally, to study hydrogen bonds and associated proton transfer, a number of spectroscopic techniques can be applied. Depending on the technique chosen, the measured observables—e.g., electronic states, molecular vibrations, or nuclear spins—are affected by dephasing and spectral diffusion on different time scales. For molecular systems in liquid solution molecular vibrations typically probe hydrogen bond dynamics with characteristics dominated by processes occurring on time scales ranging from femto- to picoseconds.[60−62] NMR on the other hand provides access to hydrogen bonds on time scales ranging from microseconds to seconds.[63−66]

Here we pursue a combined approach of experimental and theoretical IR and NMR spectroscopy to ascertain the composition of monomeric and dimeric PD and HP in weakly polar dichloromethane-d_2 solution. Using temperature-dependent ^1H NMR measurements, we estimate that below 200 K the equilibrium between monomeric and dimeric pyridone shifts almost entirely to the dimer. By use of ^{15}N-labeled pyridone we resolve the $^1J_{NH}$ coupling and confirm the structure of the dimer as cyclic $(PD)_2$. We investigate the contributions of IR-active vibrations of the different molecular species in the fingerprint and NH/OH stretching mode regions as a function of the total pyridone concentration at 300 K, and as a function of temperature between 193 and 298 K. In both regions we observe a substantial spectral overlap, preventing a straightforward assignment. To improve the spectral resolution, we apply two-dimensional correlation spectroscopy,[67,68] which provides additional insight into the assignment of absorption bands to different species by analysis of concentration- or temperature-dependent spectral changes. From the combined IR and NMR approach we conclude that PD monomer (likely complexed with a solvent molecule) and cyclic $(PD)_2$ as well as chainlike PD−PD are the most abundant species in dichloromethane-d_2 solution. The cyclic homodimer $(HP)_2$, and the cyclic heterodimer (PD−HP), as well as the HP−PD turn out to be of minor importance under steady-state conditions. Even less important are the HP monomer and chainlike PD−HP and HP−HP which are not significantly present in solution. Room temperature proton exchange rates observed with NMR spectroscopy, however, suggest that some of these species may transiently exist, facilitating routes for proton transfer between different PD units.

2. Experimental Section

2-Pyridone/2-hydroxypyridine was purchased from Fluka and used as received. 2-Pyridone/2-hydroxypridine labeled with ^{15}N was synthesized by us as described in the Supporting Information. Dichloromethane-d_2 (CD_2Cl_2) was obtained from Deutero GmbH (99.6% isotopic purity, water content <0.01%) and used unpurified for the IR measurements. A concentration-dependent series was measured with a Varian 640 FT-IR spectrometer (sample thickness 25 μm, concentration range 0.05−0.35 M). A temperature-dependent measurement on a 0.105 M pyridone solution was obtained with a Nicolet Nexus FT-IR spectrometer, using a home-built 41 μm thick cell with KRS-5 windows, placed inside a temperature-controlled jacket (Specac). CD_2Cl_2 for NMR measurements was purchased from Eurisotop GmbH, dried over molecular sieves, and transferred into the NMR sample tube via vacuum transfer. NMR spectra were measured on a Bruker AMX-500 spectrometer (500.13 MHz for ^1H, 50.68 MHz for ^{15}N), using CD_2Cl_2 as a solvent and 0.0002−0.02 M of 2-pyridone-^{15}N. Chemical shifts were measured using the solvent peak as internal standard and recalibrated into the conventional TMS scale.

Before the 2D correlation spectra were calculated, the following procedures have been applied to the set of linear IR spectra: baseline correction and subtraction of the CD_2Cl_2

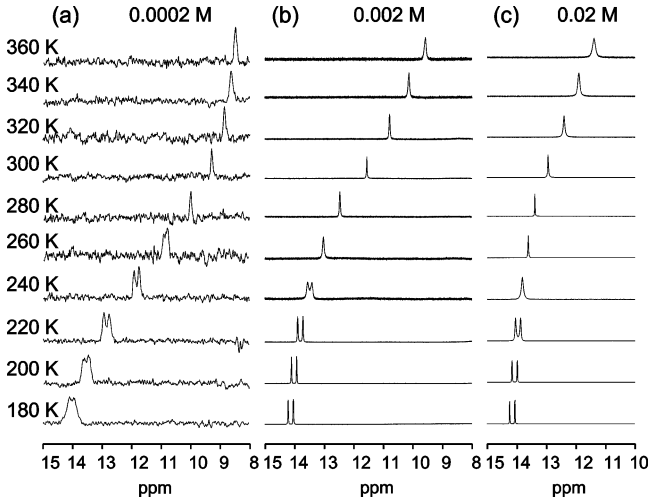

Figure 1. Low-field parts of the ^{1}H NMR spectra of pyridone-^{15}N solutions in CD_2Cl_2: (a) 0.0002 M, (b) 0.002 M, (c) 0.02 M.

solvent contributions, followed by either normalization to the total concentration (for the concentration dependent measurements) or correction for solution density changes (for the temperature-dependent experiment). The spectra were mean-centered by subtracting the average spectrum (the so-called reference spectrum). The result of this subtraction, denoted as the dynamic spectrum, represents the intensity variations at each frequency as a function of concentration. Correlations between the intensity changes are expressed as synchronous and asynchronous 2D correlation maps generated using scripts in Matlab 6.5 (The Mathworks) developed by us. These scripts are based on a modified form of the generalized 2D correlation that uses the much simpler discrete Hilbert−Noda transform of the dynamic spectra rather than the regular complex Fourier transform.[67,68] Moreover, to enhance weak spectral features, the spectra were treated with the Pareto scaling procedure prior to the final calculations of the 2D spectra.[69]

Vibrational spectra have been calculated for various monomeric and dimeric species using density functional theory (B3LYP/6-311+G(d,p)) as implemented in Gaussian 03.[70] Harmonic frequencies were obtained for optimized geometries and scaled by a factor of 0.965.

3. Experimental Results

3.1. NMR Results. We first present the results obtained by NMR spectroscopy. These spectra were recorded as a function of temperature, to investigate the possibility of slowing down proton and molecular exchange processes between the different pyridone species and resolving their corresponding NMR signals. The low-field parts of the ^{1}H NMR spectra of samples containing 0.0002, 0.002, and 0.02 M of 2-pyridone-^{15}N dissolved in CD_2Cl_2 are shown in parts a−c of Figure 1, respectively. At all temperatures only single NH signals are observed, which shifts to low field upon cooling. For all concentrations the limiting value of the chemical shift, reached at the lowest temperature, is 14.2 ppm. We have confirmed this value by measuring ^{1}H spectra of 0.02 M solution of 2-pyridone in CDF_3/CDF_2Cl mixtures at temperatures as low as 130 K (the spectra are given in the Supporting Information and the experimental technique is described in ref 71). Upon decrease of the temperature the signals decoalesce into doublets, characterized by a coupling constant of $^1J_{NH}$ = 89 Hz. The decoalescence temperature decreases from about 250 K for the 0.0002 M sample to 220 K for the 0.02 M sample. At the decoalescence temperature the inverse proton lifetime in pyridine is about 250 s^{-1}, as has been shown previously for related systems exhibiting intermolecular proton exhange from and to nitrogen.[72−74] The increase of the inverse lifetimes with concentration is a typical sign for a proton exchange mechanism involving pyridone self-associates.

TABLE 1: Experimental ^{1}H Chemical Shifts, δNH, of the Mobile Proton of 2-Pyridone-^{15}N, Dissolved in CD_2Cl_2, Obtained from Spectra Shown in Figure 1

T/K	δ(NH)/ ppm 0.0002 M	δ(NH)/ ppm 0.002 M	δ(NH)/ ppm 0.02 M
360	8.48	9.58	11.38
340	8.62	10.13	11.90
320	8.86	10.79	12.40
300	9.29	11.55	12.94
280	10.00	12.46	13.39
260	10.84	13.02	13.61
240	11.83	13.48	13.81
220	12.85	13.80	13.96
200	13.57	14.02	14.08
180	14.02	14.13	14.15

Traces of water in the samples led to a separate signal around 1 ppm at room temperature, which shifts to about 2 ppm when temperature is reduced to 200 K; further cooling leads to precipitation of the water traces as ice, no longer contributing to the spectra. Similar behavior of the residue water peak was previously reported in ref 75. The high-field parts of the spectra of the sample containing 0.02 M of pyridone dissolved in CD_2Cl_2 are shown in the Supporting Information. Thus, the exchange of the NH protons of pyridone with the OH protons of water is slow on the NMR time scale; i.e., the low-field NH resonances arise exclusively from self-associates of pyridone and proton exchange involves only the latter.

It follows that the shift of the NH signals to low field upon cooling indicates a fast molecular exchange between several pyridone species, with its equilibrium shifted to hydrogen-bonded associates upon cooling. The concentration dependence of the signals at given temperatures supports this conclusion. Experimental ^{1}H chemical shifts, δ(NH), are collected in Table 1. Their quantitative analysis and interpretation in terms of monomer−dimer equilibria are presented in the discussion section.

3.2. IR Spectra. Two spectral regions provide insight into the chemical equilibria between the pyridone species. The upper part of the fingerprint region between 1600 and 1700 cm^{-1} has C=O stretching vibrational modes indicative of PD species, either as monomer or as part of a complex. As will be shown in section 3.3, no clear marker modes are available for the HP conformer (as monomer or as constituent of a complex). In addition to that the remaining part of the fingerprint region does not provide access to distinct vibrational marker modes of particular monomer or dimer species. In the NH/OH stretching region between 2400 and 3700 cm^{-1} on the other hand both PD and HP conformers can a priori contribute, as monomer and as constituent of complexes. In parts a and b of Figure 2 we show absorption spectra for pyridone dissolved in CD_2Cl_2, normalized to the total pyridone concentration, in the frequency ranges from 1600 to 1700 cm^{-1} and 2400 to 3450 cm^{-1}. The concentration values ranging from 0.05 to 0.35 M indicate the total amount of pyridone monomer dissolved. Absorbance changes after this normalization procedure reflect differences in relative spectral contributions, caused by an altered chemical composition as a function of total pyridone concentration. The magnitude of the absorption peaks at 1618 and 1658 cm^{-1}

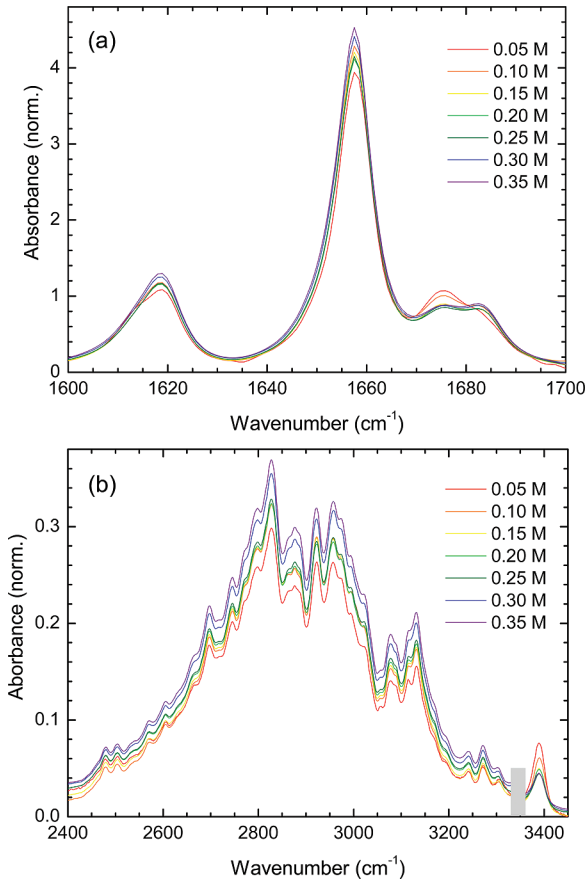

Figure 2. Concentration-dependent FT-IR spectra of PD/HP in CD_2Cl_2 after normalization to total pyridone concentration: (a) in the upper part of the fingerprint spectral region and (b) in the NH/OH stretching mode region. The gray bar around 3340 cm^{-1} indicates imperfect solvent subtraction.

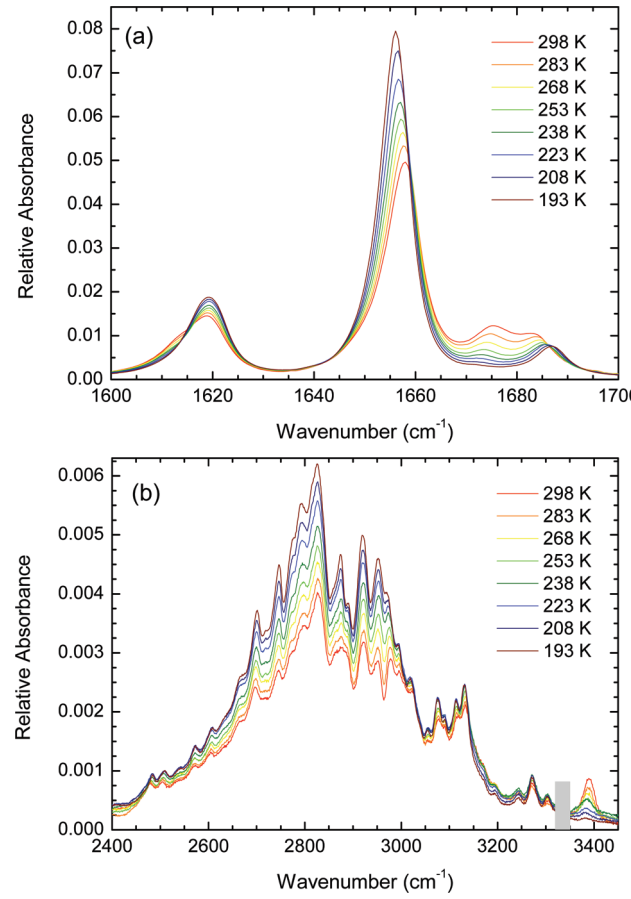

Figure 3. Temperature-dependent FT-IR spectra of PD/HP in CD_2Cl_2 after solution density correction: (a) in the upper part of the fingerprint spectral region and (b) in the NH/OH stretching mode region. The gray bar around 3340 cm^{-1} indicates imperfect solvent subtraction.

increases continuously as a function of total pyridone concentration, whereas the absorption peak at 1675 cm^{-1} changes its magnitude significantly only for the two lowest pyridone concentration values. In the NH/OH stretching region a broad absorption band containing a detailed substructure covering the range from 2400 to 3350 cm^{-1} enlarges significantly upon concentration increase, whereas a narrow band at 3391 cm^{-1} changes its magnitude in the opposite direction.

Decreasing the temperature of a 0.105 M pyridone solution from 298 to 193 K leads to a pronounced increase in magnitude of absorption bands at 1618 and 1658 cm^{-1}, where the latter shows a frequency-downshift of 2 cm^{-1}, accompanied by a band shape change (Figure 3a). In contrast, absorption bands at 1613 and 1675 cm^{-1} decrease in magnitude. The absorption band at 1675 cm^{-1} shows a frequency-downshift of 3 cm^{-1} and has fully disappeared at 193 K. The 1683 cm^{-1} band changes its magnitude to a lower value and its frequency position to a higher value (net frequency-upshift of 4 cm^{-1}). Upon temperature decrease the NH/OH stretching region depicts a clear increase of the absorption manifold between 2400 and 3000 cm^{-1}, whereas the narrow transition at 3390 cm^{-1} exhibits a decrease (Figure 3b). Interestingly the spectral region between 3000 and 3350 cm^{-1} shows less profound absorption changes with alternating positive and negative signs.

For a detailed analysis of the absorption changes of these spectrally strongly overlapping vibrational transitions as a function of concentration we use 2D IR correlation spectroscopy.[67,68] The intensity of a 2D correlation spectrum, denoted as $X(\nu_1, \nu_2)$, is equal to the cross-correlation function designed to compare the dependence patterns on parameter θ of two chosen quantities $y(\nu_1, \theta)$ and $y(\nu_2, \theta)$ measured at two different spectral variables ν_1 and ν_2

$$X(\nu_1, \nu_2) = \Phi(\nu_1, \nu_2) + i\Psi(\nu_1, \nu_2) = \frac{1}{\pi(\theta_{max} - \theta_{min})} \int_0^\infty Y_1(\Theta) \cdot Y_2(\Theta)\, d\Theta \quad (1)$$

where $Y_1(\Theta)$ is the forward Fourier transform of the spectral variation $y(\nu_1, \theta)$ observed at a given spectral variable ν_1 with respect to the external variable θ

$$Y_1(\Theta) = \int_{-\infty}^{\infty} y(\nu_1, \theta) \cdot e^{-i\Theta\theta}\, d\theta \quad (2)$$

and a similar expression holds for $Y_2(\Theta)$. In our work the external variable θ is either the total concentration of pyridone in solution or the temperature of the solution. The intensity of a synchronous 2D correlation peak $\Phi(\nu_1, \nu_2)$ represents simultaneous or coincidental changes of two separate spectral intensity variations measured at ν_1 and ν_2. In contrast, the intensity of an asynchronous spectrum $\Psi(\nu_1, \nu_2)$ represents sequential or successive instead of coincidental changes of spectral intensities. The asynchronous spectrum has no diagonal peaks, and cross peaks appear only if the intensities of the two spectral changes are noncoincident. Here, we use concentration or temperature

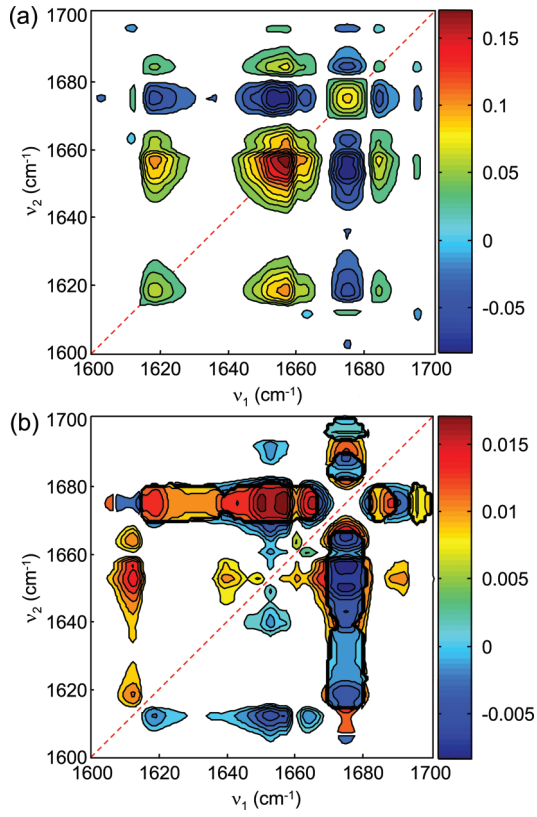

Figure 4. 2D IR correlation maps after subtracting an average spectrum and including Pareto scaling for concentration-dependent IR spectra of PD/HP in CD_2Cl_2 in the fingerprint spectral region: (a) synchronous; (b) asynchronous spectrum (multiplied by the sign of the synchronous spectrum). The color bars indicate the range of intensity values.

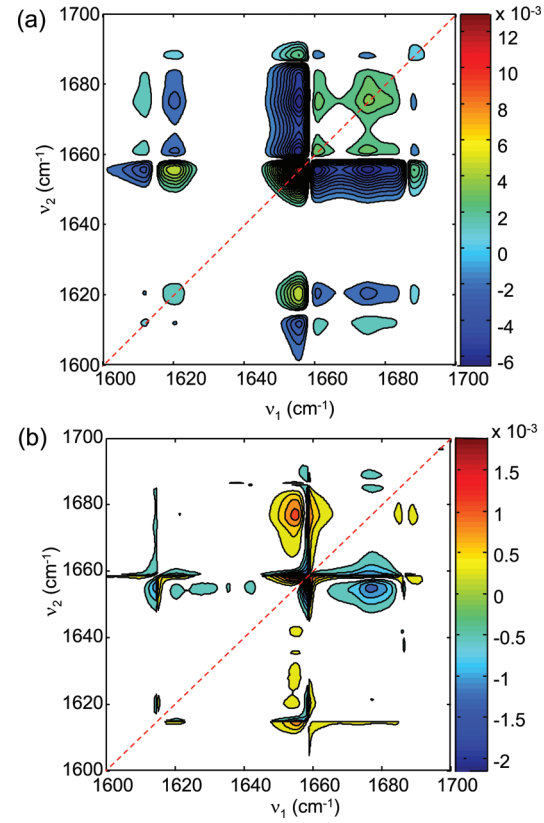

Figure 5. 2D IR correlation maps after subtracting an average spectrum and including Pareto scaling for temperature-dependent IR spectra of PD/HP in CD_2Cl_2 in the fingerprint spectral region: (a) synchronous; (b) asynchronous spectrum (multiplied by the sign of the synchronous spectrum). The color bars indicate the range of intensity values.

changes as the external perturbation θ, which shifts the equilibrium from dimeric species toward the increasingly favored formation of monomeric species upon dilution or upon heating. 2D correlation spectroscopy allows us to discern those different species by analyzing the synchronous and asynchronous maps simultaneously. In addition, the sign of asynchronous peaks provides information on the sequential order of spectral changes. We show the resulting synchronous and asynchronous 2D IR correlation maps in Figures 4 and 5 for the high-frequency part of the fingerprint spectral region, and in Figure 6 and Figure S4 for the high-frequency NH/OH stretching mode region, for the concentration-dependent and temperature-dependent experiments, respectively.

The high-frequency fingerprint range synchronous spectrum of the concentration-dependent experiment (Figure 4a) exhibits a broad diagonal peak around 1658 cm^{-1} and three other autopeaks around 1619, 1675, and 1684 cm^{-1}. Three positive off-diagonal peaks are observed at Φ(1619, 1658), Φ(1619, 1684), and Φ(1658, 1684). In addition, three negative cross peaks develop: Φ(1619, 1675), Φ(1658, 1675), and Φ(1675, 1684). The asynchronous correlation map (Figure 4b) has been multiplied by the sign of the corresponding synchronous 2D spectrum, with which Noda's rules can be applied to determine the sequential order of spectral changes. The asynchronous spectrum develops a very strong positive peak Ψ(1657, 1675). This reveals that the peaks at 1657 and 1675 originate from different species, despite the appearance of a weak synchronous peak. The sign of the peak Ψ(1675, 1687) switches between positive and negative in the center of the peak reflecting nonmonotonic spectral changes. Further positive peaks are observed at Ψ(1612, 1618), Ψ(1612, 1653), Ψ(1612, 1663), Ψ(1618, 1675), Ψ(1665, 1675). A pronounced negative peak appears at Ψ(1653, 1687).

Applying temperature as a perturbation, we generate synchronous and asynchronous 2D correlation maps of the upper part of the fingerprint region (Figure 5). Similarly to the concentration-dependent case, four diagonal peaks are present in the synchronous spectrum: one very strong autopeak at the frequency position 1656 cm^{-1} and three much weaker autopeaks located at 1619, 1675, and 1688 cm^{-1}. Three marked off-diagonal, positive peaks can be found at Φ(1619, 1656), Φ(1656, 1688) and a very weak peak at Φ(1612, 1675). In addition, there are three negative off-diagonal peaks at Φ(1612, 1656), Φ(1619, 1675), and Φ(1656, 1675). The asynchronous map (multiplied by the sign of the corresponding 2D synchronous spectrum) displays a strong positive peak at Ψ(1654, 1677). In the frequency range 1648−1662 cm^{-1} a distorted butterfly pattern is present, which, together with an angel pattern in the synchronous map, is a known characteristic of a band subject to simultaneous intensity changes and spectral shifting due to the external perturbation θ.[68]

The synchronous and asynchronous 2D correlation maps for the high-frequency NH/OH stretching mode region as a function of pyridone concentration are shown in Figure 6. The synchronous spectrum shows that the absorbance at 3390 cm^{-1} is correlated in opposite direction to all remaining changes located on its low-frequency side. Around 3340 cm^{-1} the weak peak arises due to imperfect solvent subtraction. The asynchronous map shows a strong asynchronicity for the changes at 3390 cm^{-1} and those below 3300 cm^{-1}. A second peak at 3316 cm^{-1} is asynchronous to the whole range below 3300 cm^{-1} as well. The temperature-dependent synchronous 2D correlation map for

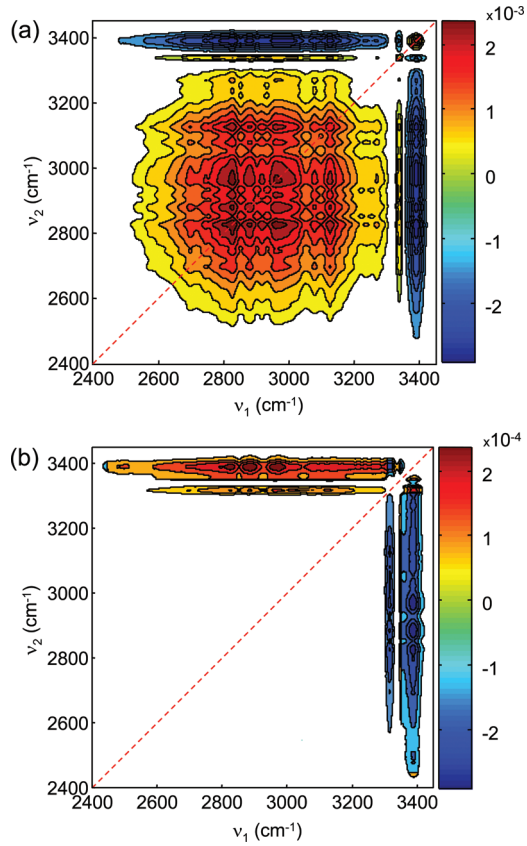

Figure 6. 2D IR correlation maps after subtracting an average spectrum and including Pareto scaling for concentration-dependent IR spectra of PD/HP in CD_2Cl_2 in the high-frequency spectral region: (a) synchronous; (b) asynchronous spectrum (multiplied by the sign of the synchronous spectrum). The color bars indicate the range of intensity values.

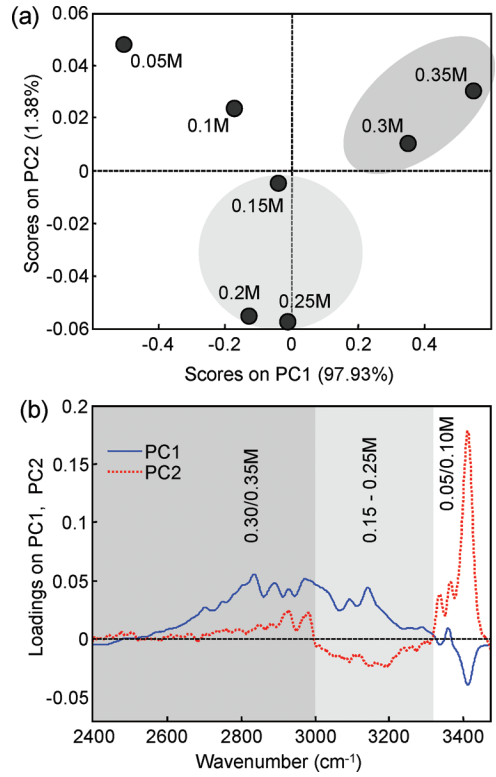

Figure 7. Principal component analysis yielding two components contributing to 97.9% (PC1) and 1.4% (PC2): (a) samples/scores plot; (b) variables/loadings plot.

the high-frequency N−H/O−H stretching mode region displays a significant positive correlation between many overlapping transitions within the 2400−3000 cm^{-1} manifold and a negative correlation of this manifold with the 3390 cm^{-1} band. In addition to that a smaller negative correlation exists with a band located at 3190 cm^{-1} (see Figure S4a in the Supporting Information). Asynchronous peaks are observed between 3000 and 3450 cm^{-1} (Figure S4b, Supporting Information).

As will be discussed later, the usefulness of 2D correlation spectroscopy in the case of a broad and structured band is limited, because the method cannot resolve many individual overlapping contributions with significantly different spectral widths. Therefore, to extract more detailed information, we applied principal component analysis (PCA).[76] This technique extracts the unique and essential information by reducing a multidimensional data set to a set of new orthogonal variables, which are called principal components. PCA decomposes the original data matrix, here the set of concentration-dependent spectra of Figure 2, as the sum of the outer product of vectors (scores) containing information on how the individual spectra relate to each other and a second set of vectors (loadings), which carry information on how the vibrational frequencies relate to each other plus a residual matrix. After smoothing the spectra with the Savitzky−Golay algorithm (filter width 25 cm^{-1}, second-order polynomial) and mean centering, two components could be extracted, one accounting for 97.93% of the absorbance changes (PC1) and the second one accounting for 1.38% (PC2), which together capture 99.32% of absorbance changes.

The scores plot in Figure 7a shows us the relationship between the spectra for the different concentrations with respect to the principal component PC1 and the second component PC2. PC1 divides the spectra into two groups of low (0.05, 0.10 M) and high (0.30, 0.35 M) concentration, whereas spectra for intermediate concentrations are close to zero on the score plot and therefore less meaningful. PC2 on the other hand, divides the spectra into one group for low and high concentrations and a second group of intermediate concentrations (0.20, 0.25 M). The corresponding loadings plot (Figure 7b) shows that the vibrational frequencies can be associated with the two principal components. For PC1, two spectral regions can be distinguished, which reflect different directions of spectral changes. The two regions are discriminated by a sign change occurring around 3300 cm^{-1}. PC2 reveals an additional spectral distinction at about 2980 cm^{-1}, which splits the broad absorption between 2400 and 3300 cm^{-1} into two parts. To conclude this section, we end up with three distinguishable spectral regions, which can be related to different concentration ranges. Changes in the highest frequency range (above ∼3300 cm^{-1}) occur mostly for the low concentration range. Changes in the low frequency range (below ∼2980 cm^{-1}) are associated with the two highest concentration values, whereas for concentrations with intermediate values spectral changes are linked to the frequency range 2980−3300 cm^{-1}.

3.3. Quantum Chemical Calculations of Vibrational Spectra. In the gas phase PD is calculated to be more stable than HP by about 310 cm^{-1}. HP is in a planar conformation where the O−H hydrogen atom points toward the side of the pyridine nitrogen atom. A conformer in which the hydrogen atom points away from the nitrogen atom (not shown) is less stable by more than 2300 cm^{-1} compared to PD. Among the three possible cyclic dimers $(PD)_2$ is the most stable one in the gas phase. $(HP)_2$ and (PD−HP) are calculated to be less stable by 1850 and 1755 cm^{-1}, respectively. A chainlike dimer, PD−PD, which is obtained from the cyclic double hydrogen-bonded dimer $(PD)_2$

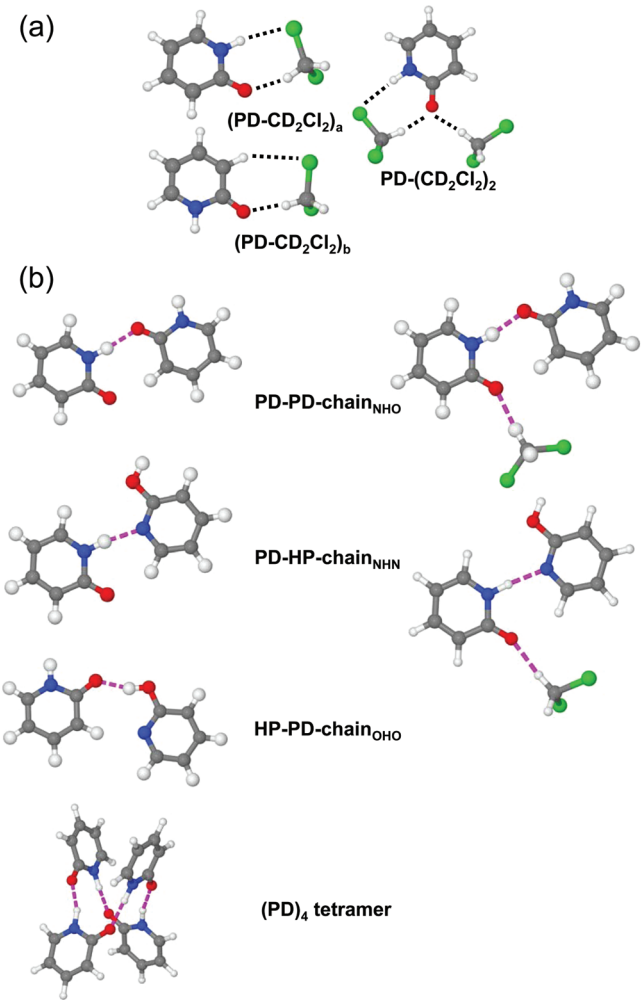

Figure 8. (a) Optimized 2-pyridone monomer complexes with one or two CD_2Cl_2 solvent molecules. (b) Optimized single hydrogen-bonded complexes unsolvated (left) and with solvated carbonyl groups with one CD_2Cl_2 solvent molecule (right); the $(PD)_4$ tetramer is shown at the bottom of the graph.

by rotating one of the monomers around the C═O bond by 180° such that they are connected only by a single hydrogen bond, is investigated as well. In addition, three different complexes between PD and one or two CD_2Cl_2 solvent molecules have been explored, as well as the cyclic tetramer $(PD)_4$ (Figure 8).

The carbonyl stretching mode ν(C═O) is quite sensitive to the local environment and might be used as a marker mode capable of distinguishing different pyridone species. In Figure 9 the experimental IR absorption spectrum of pyridone dissolved in CD_2Cl_2 is plotted in the spectral region from 1585 to 1700 cm^{-1} together with calculated peaks for different species possibly contributing to the equilibrium solution composition. The arrows denote the direction of normalized absorbance changes upon dilution. The absorption bands up to about 1630 cm^{-1} belong to N−H or O−H bending modes combined with aromatic ring stretching motions. The bands between 1630 and 1700 cm^{-1} correspond to the absorption of the C═O stretching mode. Calculated frequencies for the C═O stretching mode are summarized in Table 2. Experimentally observed frequencies in the range 1600−1700 cm^{-1} are compiled in Table 3 together with tentative assignments, which will be discussed in section 4.1. It is not possible to identify a well-isolated marker mode for HP units as monomer or as part of dimers, neither for O−H bending modes nor for C−O stretching modes, as these are located in spectral ranges of other molecular species.

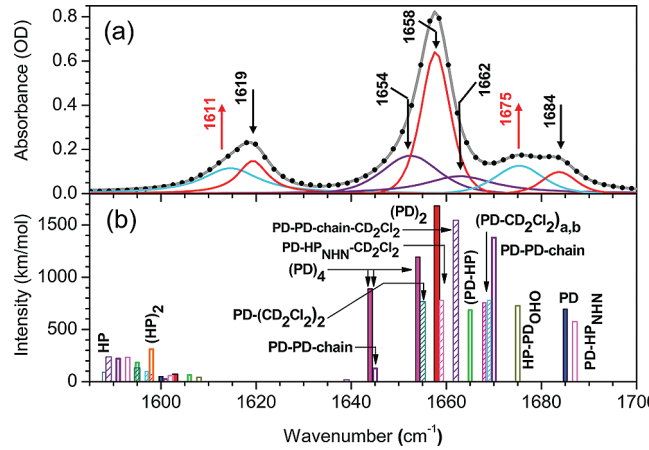

Figure 9. (a) IR absorption spectrum of 2-pyridone dissolved in CD_2Cl_2 (solid gray line) ($c = 0.20$ M) together with a peak fitting decomposition (black dots; solid colored lines depict different components) in the upper fingerprint spectral region; arrows indicate change of absorbance upon dilution. (b) Calculated peaks (B3LYP/6-311+G(d,p); scaled by 0.965) for different species (see Scheme 1 and Figure 8): 1585−1630 cm^{-1}, NH/OH bending + aromatic ring stretching vibrations; 1630−1700 cm^{-1}, C═O stretching mode absorption.

TABLE 2: Calculated Harmonic Frequencies for ν(C═O) (scaled by 0.965; in cm^{-1})

species	calculated
PD	1685
$(PD)_2$	1658
(PD−HP)	1665
$(PD-CD_2Cl_2)_a$	1668
$(PD-CD_2Cl_2)_b$	1669
$PD-(CD_2Cl_2)_2$	1655
$PD-PD\ chain_{NHO}$	1670 (s), 1645 (w)
$HP-PD\ chain_{OHO}$	1675
$PD-HP\ chain_{NHN}$	1687

4. Discussion

4.1. Equilibrium Composition of Solutions. ***4.1.1. Analysis of NMR Results.*** We start by discussing the NMR spectra, which provide first insight into the composition of the solutions. Note that at the lowest temperature used in our experiments the δ(NH) chemical shift of pyridone self-associates and approaches the value of 14.2 ppm regardless of concentration in CD_2Cl_2 and also in CDF_3/CDF_2Cl mixture. As this value is independent of concentration and the same in different polar solvents which are not hydrogen bond acceptors, we assign this value to the intrinsic value of the dominant dimer species. In addition to that, the large value of $^1J_{NH} = 89$ Hz indicates that the PD dimer structure is predominant, whereas HP can be considered to be of minor relevance.[53] This coupling constant value is typical for hydrogen bonded NH···N or NH···O hydrogen bonds,[72,77] where the value depends on the hydrogen bond strength.[78] We thus conclude that the dominant complex at low temperatures is cyclic $(PD)_2$. Indeed, the cyclic heterodimer (PD−HP) would give rise to two different H-bonding proton signals in the slow exchange regime, whereas cyclic $(HP)_2$ would have a very small value of $^1J_{NH}$.

Assuming that the temperature dependence of δ(NH) is due to a fast equilibrium between the PD (likely to exist in the form of a solute−solvent complex), and $(PD)_2$, we define the equilibrium constant K as

TABLE 3: Experimental Frequencies Observed in the Fingerprint Region in CD_2Cl_2 with Assignment (in cm^{-1}) and Calculated Counterparts

calculated	2D spectra varying temperature[a]	fitting results	assignment	species[b]
	1688 (s)	1683.5	combination tone	$(PD)_2$
1668, 1669	1675 (s)/1677 (a)	1674.9	ν(C═O)	$(PD-CD_2Cl_2)_{a,b}$
1670	1662 (a)	1661.6	ν(C═O)	PD−PD chain ($C{=}O_{free}$)
1658	1656 (s)/1658 (a)	1657.7	ν(C═O)	$(PD)_2$
1645	1654 (a)	1654.0	ν(C═O)	PD-PD-chain ($C{=}O_{HB}$)
1603	1619 (s)	1618.7	δ(NH)/ν_{ring}	$(PD)_2$
	1612 (s)	1610.9	δ(NH)/ν_{ring}	$(PD\text{-}CD_2Cl_2)_{a,b}$

[a] "s" stems from synchronous, "a" from asynchronous. [b] See Scheme 1 and Figure 6.

$$K = \exp\left(-\frac{\Delta H - T\Delta S}{RT}\right) = \frac{C_{(PD)_2}}{C_{PD}{}^2} \qquad (3)$$

$$C = C_{PD} + 2C_{(PD)_2}$$

where C_{PD} and $C_{(PD)_2}$ are the concentrations of PD and $(PD)_2$ and C is the overall concentration of PD in the solution. In the fast exchange regime the observed chemical shift is given by

$$\delta_{obs} = \frac{C_{PD}}{C}\delta_{PD} + \frac{2C_{(PD)_2}}{C}\delta_{(PD)_2} \qquad (4)$$

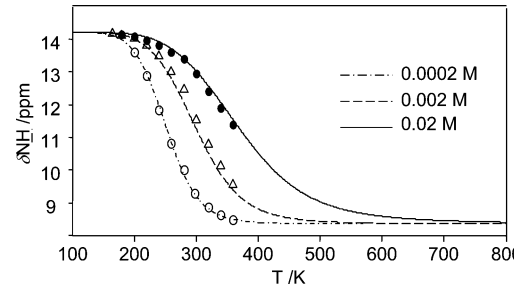

Figure 10. Averaged δ(NH) chemical shifts of pyridone solution in CD_2Cl_2 for concentrations 0.0002 M (− • − •, ○), 0.002 M (− -, △) and 0.02 M (—, ●). The fitting was done assuming the fast exchange between PD monomer and $(PD)_2$ dimer, see text for more details.

where δ_{PD} and $\delta_{(PD)_2}$ are intrinsic chemical shifts of PD and $(PD)_2$, correspondingly. Using a combination of eqs 3 and 4, the calculated chemical shifts δ(NH) represented by the different curves (Figure 10) were fitted to the experimental values using the dimerization enthalpy $\Delta H = -30.5$ kJ•mol^{-1}, the dimerization entropy $\Delta S = -50$ J•mol^{-1}•K^{-1}, and the intrinsic chemical shift of 8.4 ppm for the monomer PD. The proposed two-state equilibrium might not be valid for very high concentrations of PD as the clusters containing four or more molecules may be formed.[57,79] We conclude the analysis of the NMR results by stating that an equilibrium exists between PD monomers and cyclic $(PD)_2$ that—for temperatures well below room temperature—clearly shifts to cyclic $(PD)_2$. Here we understand PD monomers to be both free PD molecules and PD−CD_2Cl_2 complexes. The lifetime of a pyridone molecule in a dimer could not be established in this study by NMR but is sufficiently short to establish the fast monomer−dimer equilibria down to 130 K.

4.1.2. Analysis of FT-IR Results from the Fingerprint Region. Due to the time averaging aspect of NMR spectroscopy, we may be prevented from observing pyridone species with lifetimes clearly shorter than a millisecond. We thus turn to the analysis of our infrared results, which may provide access to short-lived species. In doing so, our results show both the strength and weakness of the applied IR method. We probe vibrational transitions of species-dependent marker modes in the fingerprint and in the NH/OH stretch spectral regions that indicate the presence of these species in CD_2Cl_2 solution. Interpretation of the linear spectra—together with quantum chemical calculations—to derive the chemical speciation in CD_2Cl_2 solution involves the following complications.

First, in the fingerprint region we can only identify those species that have C═O stretching marker modes, i.e., species that consist of at least one PD unit (PD monomer, PD−solvent complexes, cyclic $(PD)_2$, and cyclic (PD−HP) cyclic, and chainlike PD−PD, HD−PD, and PD−HP or even larger aggregations with at least one PD unit). In contrast, HP monomer, HP−solvent complex, cyclic $(HP)_2$ and chainlike HP−HP cannot be probed unequivocally in the fingerprint region, because OH bending motions are typically delocalized and mixed with unspecific aromatic stretching motions, which occur in all species. This is also true for C−O stretching motions, which are in addition located in the same spectral region of the C−D bending vibration of CD_2Cl_2. The strong IR absorption by the solvent makes that spectral region inaccessible.

Second, in the NH/OH stretching region only PD and HP units with their NH or OH groups not being part of a medium strong hydrogen bond (i.e., uncomplexed, or being part of a solute−solvent complex) are directly identifiable by their narrow NH or OH stretching bands. In contrast, hydrogen bond formation in dimers (in cyclic or chainlike conformations) leads to strongly broadened and red-shifted NH/OH stretching bands with pronounced substructures, revealing extensive anharmonic mode couplings of high-frequency NH/OH stretching modes with hydrogen bond low-frequency vibrations as well as fingerprint vibrations, the latter through Fermi resonance interactions with combination and overtone states. Similar characteristics have been observed in other medium−strong hydrogen-bonded molecular systems, such as formic acid dimer, acetic acid dimer, benzoic acid dimer, or 7-azaindole dimer.[80−87]

Third, a substantial spectral overlap both in the fingerprint region and in the NH/OH stretch region complicates the unique and unequivocal assignment of vibrational bands. 2D IR correlation spectroscopy, the results of which will be discussed next, has the potential to lift some of the limitations of linear IR spectroscopy.

Positive cross peaks in the synchronous correlation maps may develop if spectral changes for the two frequency positions are correlated. To confirm this correlation, cross peaks at these positions should be absent in the asynchronous maps. The strong positive cross peak around Φ(1619, 1658) appearing in the synchronous maps of the concentration- and temperature-dependent experiments (Figures 4a and 5a) together with the absence of a corresponding asynchronous peak (Figures 4b and

5b) reveals that the spectral changes at the two frequency positions are correlated and develop in the same direction. There are two more positive synchronous cross peaks without counterpart in the asynchronous spectrum in the concentration-dependent experiment, namely, the weak peaks Φ(1619, 1684) and Φ(1658, 1684), which point to some slight correlation. A similar correlation is found in the temperature-dependent synchronous map at slightly different peak positions Φ(1619, 1688) and Φ(1656, 1688). On the basis of these observations, we can state that the bands at 1619, 1658/1656, and 1684/1688 cm^{-1} are likely to originate from the same molecular species. The negative synchronous cross peaks Φ(1619, 1675), Φ(1658/1656, 1675), and Φ(1675, 1684/1688) indicate that the respective vibrational bands come from different species, because the spectral changes occur in opposite directions. A positive correlation between the 1612 and 1675 cm^{-1} bands in both experiments points to the fact that these originate from the same molecular species or associate. The concentration- and temperature-dependent synchronous maps are thus dominated by two molecular species, which are strongly negatively correlated to each other, i.e., a concentration increase or a temperature decrease leads to a rise of species I with bands at 1619, 1658/1656, and 1684/1688 cm^{-1} and a decline of species II with bands at 1612 and 1675 cm^{-1}.

In the asynchronous spectrum of the concentration-dependent experiment (Figure 4b) cross peaks at Ψ(1675, 1687) and Ψ(1612, 1618) are observed between pairs of vibrational bands assignable to different species. An even more pronounced example of improving spectral resolution is given by the temperature-dependent asynchronous map. Two strongly spectrally overlapping bands at 1654 and 1658 cm^{-1} can be distinguished by inspecting their asynchronous behavior with respect to the 1677 cm^{-1} band. This is because the 1654 cm^{-1} transition has a strong asynchronous temperature dependence compared to the 1677 cm^{-1} band, whereas the 1658 cm^{-1} transition has not and, thus, is fully absent in the asynchronous map. The asynchronicity between the two closely located bands can be also observed directly in the asynchronous spectrum at Ψ(1654, 1658). We can conclude that the strongest band of the fingerprint region is actually composed of two overlapping vibrational transitions of two distinctly different structures, namely, molecular species I (located at 1658 cm^{-1}) and a molecular species III (located at 1654 cm^{-1}), which has not been reported on previously. The same conclusion can be drawn from the concentration-dependent asynchronous map.

The analysis of the sign of the asynchronous cross peaks multiplied by the sign of the corresponding synchronous cross peaks allows us to conclude the following. On the basis of Noda's rules,[67,68] we can deduce the following sequence of the intensity variations upon temperature decrease: 1653/1654 → 1612−1675 and 1619−1658/1656−1684/1688 cm^{-1}, i.e., spectral variation of molecular species III occur before those of species I and II, where those of I and II behave in a more synchronous, but in opposite direction. We cannot draw such a straightforward conclusion from the concentration-dependent data, which may hint at the fact that concentration variation and temperature change do not necessarily imply fully identical behavior.

After having provided insight into synchronous and asynchronous correlations of different vibrational transitions, we propose assignments of the IR absorption bands (cf. Figure 9) based on the combined experimental and calculated results for the vibrational spectra. Such assignments are summarized in Table 3. We first discuss three transitions which from our 2D analysis have been shown to originate from the same molecular species I. The strong absorption band around 1658 cm^{-1}, which decreases upon dilution or heating, is assigned to absorption of the ν(C═O) mode in the cyclic homodimer $(PD)_2$, in agreement with previous assignments in the literature.[37,46] The 1619 cm^{-1} transition can be assigned to NH bending motions combined with aromatic ring stretching motions (δ(NH)/ν_{ring}) in $(PD)_2$. Because of its high transition frequency, the molecular transition located at 1684/1688 cm^{-1} cannot be due to a carbonyl stretching vibration. Instead, we suggest that this transition is caused by Fermi coupling of the carbonyl stretching vibration to either a combination tone from C−H wagging modes located around 776 and 940 cm^{-1} or a combination/overtone from a C−H wagging mode around 860 cm^{-1} and ring deformation modes around 847 cm^{-1}. These frequencies have been derived from our calculations, but we also refer to previously reported results of the similar vibrational modes in PD monomers.[44,45,54,55]

We now assign molecular species II, which has vibrational transitions at 1612 and 1675 cm^{-1}. Upon diluting/heating, the peak at 1675 cm^{-1} increases, indicating that the absorption peak is due to a monomer species that is preferentially formed at lower concentrations/higher temperatures. The results of the calculations suggest that PD−CD_2Cl_2 complexes (see Figure 8a for the two forms *a* and *b*) are responsible for the 1675 cm^{-1} band, as their ν(C═O) modes absorb in this spectral range. The 1612 cm^{-1} mode is again due to NH bending motions combined with aromatic ring stretching motions (δ(NH)/ν_{ring}).

Molecular species III, which has a spectral signature at 1653/1654 cm^{-1}, must be different from previously assigned molecular structures. The temperature-dependent asynchronous map (Figure 5b) shows an extended peak Ψ(1654−1665, 1677), which is interrupted at 1658 cm^{-1}. This could mean that a single broad transition contributes to the observed peak or it could indicate the existence of two bands with maxima at 1654 and 1662 cm^{-1}. The hydrogen-bonded PD−PD chain associates (Figure 8b) would fulfill these requirements. The peak at 1654 cm^{-1} could come from the hydrogen-bonded C═O group connecting the two PD units inside the chain dimer, whereas the peak at 1662 cm^{-1} could originate from the C═O group which likely interacts with CD_2Cl_2 solvent molecules.

On the basis of our 2D IR correlation analysis of the upper part of the fingerprint region, we can assign the molecular species I, II, and III to cyclic homodimer $(PD)_2$, the monomer−solvent complex PD−CD_2Cl_2, and the chainlike dimer−solvent complex PD−PD−CD_2Cl_2. Taking both number and position of peaks detected in the 2D synchronous and asynchronous spectra, we have applied a line shape fitting procedure using Voigt line shape functions to the IR spectrum of the 0.20 M solution. A good match between experimental and calculated spectra (Figure 9) confirms the assignment of the different spectral features. We do not need to include in this spectral range any contributions of other molecular species, including free PD monomer, chainlike PD−HP, cyclic (PD−HP), or even larger constituents, such as the symmetric cyclic tetramer $(PD)_4$.[57,79]

4.1.3. Analysis of FT-IR Results of NH/OH Stretching Region. The high-frequency IR spectrum in the range between 2400 and 3300 cm^{-1} is composed of many overlapping bands including C−H stretching modes as well as overtone and combination bands of fingerprint modes. This strong spectral overlap prevents us from obtaining an assignment of the vibrational bands with similar detail as in the fingerprint region (cf. Table 4). The absorbance in this spectral region is enhanced upon concentration increase, whereas the narrow band at 3390 cm^{-1} is decreased. Thus, we assign the broad band to dimer

TABLE 4: Experimental Frequencies $\omega/2\pi c$ Observed in the NH/OH Stretching Region in CD_2Cl_2 with Assignment (in cm^{-1})

spectral position	assignment	species[a]
3390[b]	ν(N−H)	(PD−CD_2Cl_2)$_b$ (N−H_{free}); PD−PD chain (N−H_{free})
3316[b]	ν(N−H)	(PD−CD_2Cl_2)$_a$
2980−3300[c]	ν(N−H)	PD−PD chain (N−H_{HB})
2400−2980[c]	ν(N−H)	$(PD)_2$ (N−H_{HB})

[a] See Scheme 1. [b] From asynchronous spectrum. [c] From PC analysis.

and the narrow band at higher frequency to monomer species. Accordingly, 2D analysis of the synchronous spectrum (Figure 6a) shows that the spectral changes at 3390 cm^{-1} are negatively correlated with the broad absorption band expanding from 2400 and 3300 cm^{-1}. The synchronous map obtained in the temperature experiment (Figure S4a, Supporting Information) shows the negative correlation of the 3390 cm^{-1} band with a somewhat smaller spectral range of 2650−3000 cm^{-1}. An additional peak at 3160 cm^{-1} shows a similar negative correlation with the 2650−3000 cm^{-1} manifold.

The corresponding asynchronous map in the concentration-dependent study (Figure 6b) reveals a strong asynchronicity between the peaks at 3316 and 3390 cm^{-1}, respectively, and the entire range of the broad absorption. We assign the peak at 3390 cm^{-1} to the absorption of free N−H groups in agreement with computational results and earlier studies in the literature.[19,37,44−46] The weaker asynchronous peak observed at 3316 cm^{-1} is downshifted by 74 cm^{-1} compared to the absorption of free N−H groups. According to our calculations such a red-shift accounts for N−H groups hydrogen bonded to CD_2Cl_2 solvent molecules. From the sign of the peaks it can be deduced that the changes attributed to the free N−H groups are ahead of all other changes. The 2D analysis does not allow, however, to distinguish changes, which could testify against different hydrogen-bonded dimers giving rise to the broad absorption band between 2400 and 3300 cm^{-1}.

The results obtained by PCA allow for a more detailed analysis of the high-frequency region. The scores plot (Figure 7a) shows that the first principal component (PC1) of spectral variations reflects concentration-dependent absorbance changes. Dilute samples are characterized by negative scores over PC1, whereas the concentrated solutions have opposite values. From the loadings plot (Figure 7b) it is evident that the absorbance changes are related to the absorption of free N−H groups at 3390 cm^{-1} and the broad absorption arises from dimers. Thus, PC1 is correlated with the association process as a function of concentration.

As the concentration-dependent absorbance changes (PC1) dominate (97.93%) the high-frequency spectrum, any smaller spectral variations are difficult to observe without PCA. Here, we consider a second component PC2, accounting for 1.38% of spectral variations, which shows that the broad absorbance from 2400 to 3300 cm^{-1} arises from two differently associated species. From the simultaneous analysis of scores and loadings plots we assign that the high concentrations—where scores vs PC1 and PC2 are positive—have the biggest influence on spectral variations in the range from 2400 to 2980 cm^{-1}, where in addition the loadings against the two components are positive. From this we derive that absorbance of the hydrogen-bonded N−H stretching band of cyclic $(PD)_2$ must dominate this spectral region. The intermediate concentrations, instead, have the largest influence on the spectral variations in the range from 2980 to 3300 cm^{-1}. Therefore, we attribute absorption in this range to species exhibiting weaker hydrogen bonds as compared to the cyclic dimer. For instance, single hydrogen-bonded chain dimers could account for absorption in this range. It should be noted that the small contribution of PC2 to the spectral changes does not allow us to form a conclusion on the relative concentrations of different species in solution.

The PCA results are independently supported by analysis of the temperature-dependent linear spectra in the NH/OH stretching region (Figure 3b). In the range between 2400 and 3000 cm^{-1} the broad spectral manifold increases clearly in magnitude upon cooling, the transitions between 3000 and 3300 cm^{-1} show less change in absorbance, and the 3390 cm^{-1} band decreases in magnitude.

We summarize our work on the IR spectra by concluding that the marker bands of the fingerprint region provide evidence for the existence of cyclic $(PD)_2$ and PD−CD_2Cl_2 solute−solvent complexes, with an additional component assigned to chainlike PD−PD. The NH/OH stretching region shows vibrational marker bands that are assigned to uncomplexed NH groups (by PD monomers and/or PD units being part of chain-like dimers), and to PD−CD_2Cl_2 solute−solvent complexes. We did not observe uncomplexed OH stretching marker bands of the HP monomer and chainlike PD−HP and HP−HP. Extensive spectral overlap prevents a clear assignment of the broad spectral band between 2400 and 3300 cm^{-1} to a single hydrogen-bonded species. Our 2D and PC analysis suggests strongly that this spectral region has three components, which would be in accordance with our assignment of the fingerprint region.

4.2. Exchange Mechanisms on Long Time Scales. As can be seen from Figure 1, at temperatures above 240 K the doublet due to the $^1J_{NH}$ coupling constant in PD collapses. This indicates the onset of an intermolecular proton exchange between different PD units, which is fast on the NMR time scale. In Scheme 2 we are showing a set of the reactions which are important for the discussion of the proton exchange mechanism. Scheme 2a−c shows the formation of cyclic dimers $(PD)_2$, $(HP)_2$, and (PD−HP) from the corresponding monomers. We understand that the breaking and formation of the cyclic dimers likely occur via the pathways involving chainlike open dimers, the latter may act as transient or a short-lived species, where short-lived species has a lifetime much shorter than the NMR time scale, estimated to be a millisecond in this case. However, we omit the open-chain structures from Scheme 2 for clarity purposes. Scheme 2d shows the double proton transfer which converts $(PD)_2$ into $(HP)_2$. The direct intramolecular conversion of PD monomers into HP monomers is unlikely because of the high energy barrier for such a process.[48] The more probable conversion via the double proton transfer within the cyclic dimer is indirectly supported by the spectra of pyridone solutions in CD_2Cl_2 in the presence of $SbCl_5$; see Supporting Information for spectra and interpretation. Scheme 2e shows the degenerate double proton transfer reaction which interconverts cyclic (PD−HP) and cyclic (HP−PD).

The proton exchange mechanism consists of several steps and starts with the appropriate PD and HP monomers. Analysis given in Figure 10 indicates that at low concentration and high temperatures there is a significant fraction of pyridone mono-

mers, while at lowest temperatures the formation of monomers would require breakage of a dimer. The dimers are mostly in the $(PD)_2$ form, so the HP monomers are created if the $(PD)_2$ converts into $(HP)_2$ by the double proton transfer prior to the breaking. The proton exchange proceeds when PD and HP monomers form a heterodimer (PD−HP), which converts into (HP−PD) by another double proton transfer. Eventually the heterodimer breaks back into monomers, which can further participate in the formation of the dimers and continuation of the proton exchange.

5. Conclusion

In summary, even though a priori the isomerization and association chemistry of 2-pyridone/2-hydroxypyridine involves a complex set of equilibria, including monomers, solute−solvent complexes, and cyclic and open chainlike dimers, we are able to make specific statements when using dichloromethane-d_2 as solvent. By applying both NMR and FT-IR spectroscopy, we clearly identify the existence of PD−CD_2Cl_2, and cyclic $(PD)_2$ in solution. The NMR results show that the cyclic dimer $(PD)_2$ is the dominant species at low temperatures (180 K), which exchanges with PD in monomer form or complexed with the solvent. At low temperature (193 K) the IR spectra support the NMR conclusions that the solution composition is dominated by cyclic $(PD)_2$. The 2D IR correlation spectra not only show the existence of PD−CD_2Cl_2 solute−solvent complexes, and of cyclic $(PD)_2$, but also hint at the presence of chainlike PD−PD as well. At room temperature the presence of the proton exchange between PD units is inferred from the NMR spectra. We suggest certain routes for proton transfer observed on the NMR time scale, including (PD−HP) and $(HP)_2$. The fact that these complexes do not significantly show up in the IR spectra indicates that the relative concentration must be minor and their average lifetimes much shorter than milliseconds.

Acknowledgment. This work has benefited from financial support by the Deutsche Forschungsgemeinschaft (including SFB450-B2) and the Fonds der Chemischen Industrie. We cordially thank Professor Dr. Maria Rospenk and Dr. Olaf Czupiński from University of Wrocław for their assistance in the temperature-dependent IR experiment.

Supporting Information Available: Description of synthesis of 2-pyridone-^{15}N, ^{1}H NMR spectra of 2-pyridone solutions in CD_2Cl_2 in the presence of $SbCl_5$, high-field parts of ^{1}H NMR spectra of 0.02 M pyridone solutions in CD_2Cl_2, ^{1}H NMR spectra of 2-pyridone-^{14}N solution in CDF_3/CDF_2Cl at low temperature, and 2D correlation spectra of the NH/OH stretching region derived from temperature-dependent experiments. This material is available free of charge via the Internet at http://pubs.acs.org.

References and Notes

(1) Hobza, P.; Šponer, J. *Chem. Rev.* **1999**, *99*, 3247.
(2) Nir, E.; Kleinermanns, K.; de Vries, M. S. *Nature* **2000**, *408*, 949.
(3) Zoete, V.; Meuwly, M. *J. Chem. Phys.* **2004**, *121*, 4377.
(4) Bakker, J. M.; Compagnon, I.; Meijer, G.; von Helden, G.; Kabeláč, M.; Hobza, P.; de Vries, M. S. *Phys. Chem. Chem. Phys.* **2004**, *6*, 2810.
(5) Nir, E.; Hünig, I.; Kleinermanns, K.; de Vries, M. S. *ChemPhysChem* **2004**, *5*, 131.
(6) Abo-Riziq, A.; Grace, L.; Nir, E.; Kabelac, M.; Hobza, P.; de Vries, M. S. *Proc. Natl. Acad. Sci. U.S.A.* **2005**, *102*, 20.
(7) de Vries, M. S.; Hobza, P. *Annu. Rev. Phys. Chem.* **2007**, *58*, 585.
(8) Céron-Carrasco, J. P.; Requena, A.; Zúñiga, J.; Michaux, C.; Perpète, E. A.; Jacquemin, D. *J. Phys. Chem. A* **2009**, *113*, 10549.
(9) Céron-Carrasco, J. P.; Requena, A.; Michaux, C.; Perpète, E. A.; Jacquemin, D. *J. Phys. Chem. A* **2009**, *113*, 7892.
(10) Taylor, C. A.; El-Bayoumi, M. A.; Kasha, M. *Proc. Natl. Acad. Sci. U.S.A.* **1969**, *63*, 253.
(11) Douhal, A.; Kim, S. K.; Zewail, A. H. *Nature* **1995**, *378*, 260.
(12) Müller, A.; Talbot, F.; Leutwyler, S. *J. Am. Chem. Soc.* **2002**, *124*, 14486.
(13) Wu, R.; Brutschy, B. *J. Phys. Chem. A* **2004**, *108*, 9715.
(14) Roscioli, J. R.; Pratt, D. W. *Proc. Natl. Acad. Sci. U.S.A.* **2003**, *100*, 13752.
(15) Beak, P.; Fry, F. S., Jr. *J. Am. Chem. Soc.* **1973**, *95*, 1700.
(16) Beak, P.; Fry, F. S., Jr.; Lee, J.; Steele, F. *J. Am. Chem. Soc.* **1976**, *98*, 171.
(17) Brown, R. S.; Tse, A.; Vederas, J. C. *J. Am. Chem. Soc.* **1980**, *102*, 1174.
(18) Nimlos, M. R.; Kelley, D. F.; Bernstein, E. R. *J. Phys. Chem.* **1989**, *93*, 643.
(19) Matsuda, Y.; Ebata, T.; Mikami, N. *J. Chem. Phys.* **1999**, *110*, 8397.
(20) Matsuda, Y.; Ebata, T.; Mikami, N. *J. Chem. Phys.* **2000**, *113*, 573.
(21) Florio, G. M.; Gruenloh, C. J.; Quimpo, R. C.; Zwier, T. S. *J. Chem. Phys.* **2000**, *113*, 11143.
(22) Sakota, K.; Tokuhara, S.; Sekiya, H. *Chem. Phys. Lett.* **2007**, *448*, 159.
(23) Hazra, M. K.; Chakraborty, T. *J. Phys. Chem. A* **2008**, *112*, 1100.
(24) Hazra, M. K.; Samanta, A. K.; Chakraborty, T. *J. Chem. Phys.* **2006**, *125*, 214302.
(25) Penfold, B. R. *Acta Crystallogr.* **1953**, *6*, 591.
(26) Yang, H. W.; Craven, B. M. *Acta Crystallogr., Sect. B* **1998**, *54*, 912.
(27) Arman, H. D.; Poplaukhin, P.; Tiekink, E. R. T. *Acta Crystallogr., Sect. E* **2009**, *65*, 03187.
(28) Müller, A.; Talbot, F.; Leutwyler, S. *J. Chem. Phys.* **2000**, *112*, 3717.
(29) Müller, A.; Talbot, F.; Leutwyler, S. *J. Chem. Phys.* **2001**, *115*, 5192.
(30) Müller, A.; Talbot, F.; Leutwyler, S. *J. Chem. Phys.* **2002**, *116*, 2836.
(31) Borst, D. R.; Roscioli, J. R.; Pratt, D. W.; Florio, G. M.; Zwier, T. S.; Müller, A.; Leutwyler, S. *Chem. Phys.* **2002**, *283*, 341.
(32) Meuwly, M.; Müller, A.; Leutwyler, S. *Phys. Chem. Chem. Phys.* **2003**, *5*, 2663.
(33) Frey, J. A.; Leist, R.; Tanner, C.; Frey, H.-M.; Leutwyler, S. *J. Chem. Phys.* **2006**, *125*, 114308.
(34) Hammes, G. G.; Spivey, H. O. *J. Am. Chem. Soc.* **1966**, *88*, 1621.
(35) Hammes, G. G.; Lillford, P. J. *J. Am. Chem. Soc.* **1970**, *92*, 7578.
(36) Beak, P. *Acc. Chem. Res.* **1977**, *10*, 186.
(37) Bensaude, O.; Chevrier, M.; Dubois, J. E. *J. Am. Chem. Soc.* **1978**, *100*, 7055.
(38) Rawson, J. M.; Winpenny, R. E. P. *Coord. Chem. Rev.* **1995**, *139*, 313.
(39) Chou, P.-T.; Wei, C.-Y.; Hung, F.-T. *J. Phys. Chem. B* **1997**, *101*, 9119.
(40) Frank, J.; Katritzky, A. R. *J. Chem. Soc., Perkin Trans. 2* **1976**, 1428.
(41) Bensaude, O.; Chevrier, M.; Dubois, J.-E. *Tetrahedron Lett.* **1978**, *19*, 2221.
(42) Forlani, L.; Cristoni, G.; Boga, C.; Todesco, P. E.; Del Vecchio, E.; Selva, S.; Monari, M. *ARKIVOC* **2002**, *XI*, 198.
(43) Smets, J.; Maes, G. *Chem. Phys. Lett.* **1991**, *187*, 532.
(44) Nowak, M. J.; Lapinski, L.; Fulara, J.; Les, A.; Adamowicz, L. *J. Phys. Chem.* **1992**, *96*, 1562.
(45) Dkhissi, A.; Houben, L.; Smets, J.; Adamowicz, L.; Maes, G. *J. Mol. Struct.* **1999**, *484*, 215.
(46) Abdulla, H. I.; El-Bermani, M. F. *Spectrochim. Acta, Part A* **2001**, *57*, 2659.
(47) De Kowalewski, D. G.; Contreras, R. H.; Díez, E.; Esteban, A. *Mol. Phys.* **2004**, *102*, 2607.
(48) Moreno, M.; Miller, W. H. *Chem. Phys. Lett.* **1990**, *171*, 475.
(49) Wang, J.; Boyd, R. J. *J. Phys. Chem.* **1996**, *100*, 16141.
(50) Alkorta, I.; Elguero, J. *J. Org. Chem.* **2002**, *67*, 1515.
(51) Wolfe, S.; Weinberg, N.; Hsieh, Y. *Theor. Chem. Acc.* **2007**, *118*, 265.
(52) Beak, P.; Covington, J. B.; Smith, S. G. *J. Am. Chem. Soc.* **1976**, *98*, 8284.
(53) Coburn, R. A.; Dudek, G. O. *J. Phys. Chem.* **1968**, *72*, 1177.
(54) Kwiatkowski, J. S.; Leszczynski, J. *J. Mol. Struct.* **1996**, *376*, 325.
(55) Kwiatkowski, J. S.; Leszczyński, J. *J. Mol. Struct.: THEOCHEM* **1994**, *312*, 201.
(56) Müller, A.; Losada, M.; Leutwyler, S. *J. Phys. Chem. A* **2004**, *108*, 157.
(57) Motley, T. L.; Korter, T. M. *Chem. Phys. Lett.* **2008**, *464*, 171.
(58) Wójcik, M. J.; Tatara, W.; Boczar, M.; Apola, A.; Ikeda, S. *J. Mol. Struct.* **2001**, *596*, 207.
(59) Thanopulos, I.; Shapiro, M. *J. Am. Chem. Soc.* **2005**, *127*, 14434.
(60) Nibbering, E. T. J.; Elsaesser, T. *Chem. Rev.* **2004**, *104*, 1887.

(61) Woutersen, S.; Mu, Y.; Stock, G.; Hamm, P. *Chem. Phys.* **2001**, *266*, 137.
(62) Zheng, J.; Kwak, K.; Asbury, J.; Chen, X.; Piletic, I. R.; Fayer, M. D. *Science* **2005**, *309*, 1338.
(63) Golubev, N. S.; Smirnov, S. N.; Tolstoy, P. M.; Sharif, S.; Toney, M. D.; Denisov, G. S.; Limbach, H. H. *J. Mol. Struct.* **2007**, *844*, 319.
(64) Fürtig, B.; Buck, J.; Manoharan, V.; Bermel, W.; Jäschke, A.; Wenter, P.; Pitsch, S.; Schwalbe, H. *Biopolymers* **2007**, *86*, 360.
(65) Noble, D. L.; Aibout, A.; Horsewill, A. J. *J. Magn. Reson.* **2009**, *201*, 157.
(66) Lopez del Amo, J. M.; Langer, U.; Torres, V.; Pietrzak, M.; Buntkowsky, G.; Vieth, H.-M.; Shibl, M. F.; Kühn, O.; Bröring, M.; Limbach, H.-H. *J. Phys. Chem. A* **2009**, *113*, 2193.
(67) Noda, I. *Appl. Spectrosc.* **1993**, *47*, 1329.
(68) Noda, I.; Ozaki, Y. *Two-Dimensional Correlation Spectroscopy*; John Wiley & Sons: Chicester, 2004.
(69) Noda, I. *J. Mol. Struct.* **2008**, *883*, 216.
(70) Frisch, M. J.; Trucks, G. W.; Schlegel, H. B.; Scuseria, G. E.; Robb, M. A.; Cheeseman, J. R.; Zakrzewski, V. G.; Montgomery, J. A.; Stratmann, R. E.; Burant, J. C.; Dapprich, S.; Millam, J. M.; Daniels, A. D.; Kudin, K. N.; Strain, M. C.; Farkas, O.; Tomasi, J.; Barone, V.; Cossi, M.; Cammi, R.; Mennucci, B.; Pomelli, C.; Adamo, C.; Clifford, S.; Ochterski, J.; Petersson, G. A.; Ayala, P. Y.; Cui, Q.; Morokuma, K.; Malick, D. K.; Rabuck, A. D.; Raghavachari, K.; Foresman, J. B.; Cioslowski, J.; Ortiz, J. V.; Stefanov, B. B.; Liu, G.; Liashenko, A.; Piskorz, P.; Komaromi, I.; Gomperts, R.; Martin, R. L.; Fox, D. J.; Keith, T.; Al-Laham, M. A.; Peng, C. Y.; Nanayakkara, A.; Gonzalez, C.; Challacombe, M.; Gill, P. M. W.; G. Johnson, B.; Chen, W.; Wong, M. W.; Andres, J. L.; Head-Gordon, M.; Replogle, E. S.; Pople, J. A. *Gaussian 03 (Revision C.02)*; Gaussian, Inc.: Pittsburgh, PA, 2003.
(71) Tolstoy, P. M.; Schah-Mohammedi, P.; Smirnov, S. N.; Golubev, N. S.; Denisov, G. S.; Limbach, H.-H. *J. Am. Chem. Soc.* **2004**, *126*, 5621.
(72) Meschede, L.; Gerritzen, D.; Limbach, H.-H. *Ber. Bunsen-Ges. Phys. Chem. Chem. Phys.* **1988**, *92*, 469.
(73) Meschede, L.; Limbach, H.-H. *J. Phys. Chem.* **1991**, *95*, 10267.
(74) Limbach, H.-H.; Männle, F.; Detering, C.; Denisov, G. S. *Chem. Phys.* **2005**, *319*, 69.
(75) Nakahara, M.; C., W. *Chem. Lett.* **1992**, 809.
(76) Jackson, J. E. *A User's Guide to Principal Components*; John Wiley & Sons: New York, 1991.
(77) Rüterjans, H.; Kaun, E.; Hull, W. E.; Limbach, H.-H. *Nucleic Acids Res.* **1982**, *10*, 7027.
(78) Limbach, H.-H.; Pietrzak, M.; Sharif, S.; Tolstoy, P. M.; Shenderovich, I. G.; Smirnov, S. N.; Golubev, N. S.; Denisov, G. S. *Chem.—Eur. J.* **2004**, *10*, 5195.
(79) Motley, T. L.; Allis, D. G.; Korter, T. M. *Chem. Phys. Lett.* **2009**, *478*, 166.
(80) Florio, G. M.; Sibert, E. L.; Zwier, T. S. *Faraday Discuss.* **2001**, *118*, 315.
(81) Häber, T.; Schmitt, U.; Emmeluth, C.; Suhm, M. A. *Faraday Discuss.* **2001**, *118*, 331.
(82) Florio, G. M.; Zwier, T. S.; Myshakin, E. M.; Jordan, K. D.; Sibert, E. L., III *J. Chem. Phys.* **2003**, *118*, 1735.
(83) Emmeluth, C.; Suhm, M. A. *Phys. Chem. Chem. Phys.* **2003**, *5*, 3094.
(84) Emmeluth, C.; Suhm, M. A.; Luckhaus, D. *J. Chem. Phys.* **2003**, *118*, 2242.
(85) Antony, J.; von Helden, G.; Meijer, G.; Schmidt, B. *J. Chem. Phys.* **2005**, *123*, 014305.
(86) Dreyer, J. *J. Chem. Phys.* **2005**, *122*, 184306.
(87) Dreyer, J. *J. Chem. Phys.* **2007**, *127*, 054309.

JP103630W